TITLE: Pre-existing immunity drives the response to neoadjuvant chemotherapy in esophageal adenocarcinoma

Giuseppina Arbore[1,2†], Luca Albarello[3], Gabriele Bucci[4], Marco Punta[4,5], Andrea Cossu[6], Lorella Fanti[7], Aurora Maurizio[4], Francesco Di Mauro[1], Vito Bilello[1], Gianluigi Arrigoni[3], Silvia Bonfiglio[4], Donatella Biancolini[4], Francesco Puccetti[2,6], Ugo Elmore[2,6], Luca Vago[5,2], Stefano Cascinu[2,8], Giovanni Tonon[2,4], Riccardo Rosati[2,6], Giulia Casorati[1*†], Paolo Dellabona[1*†]

1 Experimental Immunology Unit, IRCCS San Raffaele Scientific Institute, Milan, Italy
2 Vita-Salute San Raffaele University, Milan, Italy
3 Department of Pathology, IRCCS San Raffaele Scientific Institute, Milan, Italy
4 Center for OMICS Sciences, IRCCS San Raffaele Scientific Institute, Milan, Italy
5 Hematology and Bone Marrow Transplant Unit, IRCCS San Raffaele Scientific Institute, Milan, Italy
6 Department of Gastrointestinal Surgery, IRCCS San Raffaele Scientific Institute, Milan, Italy
7 Division of Gastroenterology & Gastrointestinal Endoscopy, San Raffaele Scientific Institute, Milan, Italy.
8 Department of Oncology, IRCCS San Raffaele Scientific Institute, Milan, Italy
* These authors contributed equally
† Co-corresponding authors

Running Title: Esophagus adenocarcinoma neoadjuvant chemotherapy immunity

Corresponding Authors:
Giuseppina Arbore, IRCCS San Raffaele Scientific Institute, Via Olgettina 58, 20132, Milan, Italy, +39-226434735, arbore.giuseppina@hsr.it
Paolo Dellabona, IRCCS San Raffaele Scientific Institute, Via Olgettina 58, 20132, Milan, Italy, +39-226434727, dellabona.paolo@hsr.it
Giulia Casorati, IRCCS San Raffaele Scientific Institute, Via Olgettina 58, 20132, Milan, Italy, +39-226434727, casorati.giulia@hsr.it

The authors declare no potential conflicts of interest.

ABSTRACT

Current treatment for patients with locally advanced esophageal adenocarcinoma (EAC) is neoadjuvant chemotherapy (nCT), alone or combined with radiotherapy, before surgery. However, fewer than 30% of treated patients show a pathological complete response to nCT, which correlates with increased 5-year survival compared to non-responders. Understanding the mechanisms of response to nCT is pivotal to better stratify patients and inform more efficacious therapies. Here, we investigated the immune mechanisms involved in nCT response by multi-

dimensional profiling of pre-treatment tumor biopsies and blood from 68 EAC patients (34 prospectively and 34 retrospectively collected), comparing complete responders versus non-responders to nCT. At the tumor level, complete response to nCT was associated with molecular signatures of immune response and proliferation, increased putative anti-tumor tissue-resident memory $CD39^{+}CD103^{+}CD8^{+}$ T cells and reduced immunosuppressive T regulatory cells and M2-like macrophages. Systemically, complete responders showed higher frequencies of immunostimulatory $CD14^{+}CD11c^{+}$HLA-DR^{high} cells and reduced $PDL1^{+}$ monocytic myeloid-derived suppressor cells, along with high plasma GM-CSF (pro-inflammatory) and low IL-4, CXCL10, C3a, and C5a (suppressive). Plasma pro-inflammatory and suppressive cytokines correlated directly and inversely, respectively, with the frequency of tumor-infiltrating $CD39^{+}CD103^{+}CD8^{+}$ T cells. These results suggest that pre-existing immunity in baseline tumors drives the clinical activity of nCT in locally advanced EAC. Furthermore, it may be possible to stratify patients based on predictive immune signatures, enabling tailored neoadjuvant and/or adjuvant regimens.

STATEMENT OF SIGNIFICANCE

Multi-dimensional profiling of pre-treatment esophageal adenocarcinoma shows patient response to neoadjuvant chemotherapy is correlated with active pre-existing immunity and indicates molecular pathways of resistance that may be targeted to improve clinical outcomes.

INTRODUCTION

Esophageal cancer is the sixth most common cause of global cancer-associated deaths worldwide (1). Esophageal adenocarcinoma (EAC), its pathological variant, is the predominant subtype in Western countries, which have seen a sharp increase in its incidence over the past four decades (1). EAC typically affects the distal esophagus near the gastric junction; it is associated with obesity, gastroesophageal reflux, and a precursor condition known as Barrett's esophagus (1). EAC is characterized by high tumor mutational burden (TMB), large-scale chromosomal instability, and genomic structural alterations, which contribute to a poor prognosis with less than 20% of patients surviving beyond 5 years (1). Most EAC patients are diagnosed with locally advanced disease, which invades local tissues or involves regional lymph nodes without distant metastases (AJCC stage ≥T2 or N+, M0). To reduce tumor bulk and improve survival, neoadjuvant (preoperative) chemotherapy (nCT), either alone or in combination with radiation therapy, is recommended for all locally advanced cases, followed by radical surgery (1-3). However, only about 30% of treated patients show a pathological complete response with tumor and/or lymph node downstaging, which is associated with a 5-year survival rate of 64% in responders compared to 18% in non-responders (1-2). Nevertheless, the mechanisms underlying EAC response to nCT remain largely undefined. Consequently, identifying predictors of response could improve patient stratification and inform the design of more efficacious neoadjuvant and/or adjuvant therapies, which may increase response rates without subjecting patients to unnecessary treatments.

Effective cancer control depends on active immune surveillance, particularly by tumor-reactive T cells. The presence of tumor-infiltrating T lymphocytes (TILs) has also been associated with better prognosis in several malignancies (4). Non-synonymous somatic DNA mutations in cancer cells generate unique tumor neoantigens that serve as strong targets for cancer-reactive T cells (5). However, tumor-specific T cell immunity is often suppressed by several mechanisms that can be effectively targeted by therapies to restore efficient disease control. For instance, immunotherapy using monoclonal antibodies (mAb) to block inhibitory immune checkpoint molecules has been successfully employed in reinstating T cell functions (6). In addition, the efficacy of conventional chemotherapy and radiotherapy is not solely dependent on the direct effects of antineoplastic agents or radiation on cancer cells but also on the stimulation of the host immune system, which is ultimately responsible for eliminating the tumor and the ensuing long-lasting clinical effects (7, 8). Indeed, both the antineoplastic drugs (e.g., platinum derivatives, 5-fluorouracil, taxanes) and radiation utilized in nCT protocols for EAC are capable of inducing immunogenic cancer cell death, which, in turn, stimulates the tumor-specific immune response and/or has direct immunomodulatory effects (7-9).

Given these perspectives, it remains unknown whether the pathological complete response attained by preoperative treatments in a subset of EAC patients is driven by immunoreactive tumor microenvironment (TME), which stimulates the tumor-specific T lymphocyte response and contributes to cancer cell elimination. To examine this hypothesis, molecular and immune profiling of the TME in EAC needs to be performed to assess the baseline composition of the TME prior to therapy. However, there is a lack of such data in the literature. Thus, in this study, we

performed deep multidimensional profiling of baseline (i.e., pre-treatment) tumor biopsies and paired baseline blood samples to unravel the immune determinants that might contribute to the variability in treatment response to nCT.

MATERIALS AND METHODS

Study design

All samples analyzed in this study were collected from EAC patients diagnosed with a locally advanced tumor (AJCC stage ≥T2 or N+, M0), who received treatment at San Raffaele Research Hospital between 2014 and 2021. All samples were collected at baseline (i.e., before patients received treatment). The study leveraged prospective and retrospective patient cohorts (Supplementary Figure 1). The Institutional Ethics Committee approved the prospective observational study (protocol ESO-CA001), which was conducted at San Raffaele Research Hospital (OSR) in Milan, Italy. The San Raffaele Hospital Oncology board made therapy decisions based on patients' clinical condition and the current European Society for Medical Oncology (ESMO) Clinical Practice Guideline for esophageal cancer treatment (3). Written informed consent was obtained from all patients of the prospective cohort (n=34) (Supplementary Table 1), including the collection and analysis of endoscopy biopsies of tumor tissue (6-8 biopsies per patient) and blood samples (50 mL). Whole exome sequencing (WES), bulk RNA sequencing (RNA-seq), immunohistochemistry (IHC), digital spatial tissue profiling (DSP), and high-dimensional flow cytometry were performed to analyze tumor samples. Plasma was isolated from blood supernatant and frozen at -80°C, while peripheral blood mononuclear cells (PBMCs) were obtained by Ficoll separation (Ficoll-Paque PLUS, GE Healthcare Bio-Sciences). Pre-treatment tumor biopsies were freshly frozen in

OCT (n=4 biopsies per patient) for genomic analysis. For flow cytometry analysis, 2–4 EAC biopsies were dissociated in RPMI media (Gibco) using the GentleMACS (Miltenyi) Dissociator and human tumor dissociation kit. After surgery, two expert gastrointestinal pathologists, who were blinded to the clinical data, assessed the post-nCT pathological response status by examining surgical resections.

In addition to the prospective patient cohort, archived clinically annotated baseline EAC biopsies from a second independent retrospective cohort of patients were analyzed to increase the sample size for the IHC and DSP analyses. These samples were available at San Raffaele Hospital (n=34; protocols DSAN 718/1F and DSAN 0565/5TF) and are detailed in Supplementary Table 2. The archived tumor material was formalin-fixed and paraffin-embedded, making it suitable for tissue studies but unsuitable for transcriptional analysis due to insufficient RNA quality compared to freshly frozen prospectively collected tumor biopsies.

Both patient cohorts (Supplementary Tables 1 and 2) underwent neoadjuvant chemotherapy with platinum derivatives, alone or in combination with radiotherapy, mainly following the treatment protocols FLOT (combining the drugs fluorouracil, leucovorin, oxaliplatin, and docetaxel) and CROSS (combining the drugs carboplatin and paclitaxel with radiotherapy at 41.4 Gy given in 23 fractions). The studies were conducted in accordance with the Declaration of Helsinki and were approved by the San Raffaele Ethics Committee.

Whole exome and RNA sequencing

WES and RNA-seq were performed on treatment-naïve EACs. To mitigate the elevated heterogeneity described for EAC (1), 3–4 biopsies that sampled different areas of each tumor were pooled before being subjected to nucleic acid extraction. Next, freshly frozen EAC biopsies were sectioned for DNA and RNA extraction, while two adjacent sections were evaluated by hematoxylin and eosin staining to determine the tumor content (>70% for sequencing). Genomic DNA and total RNA were extracted using the AllPrep DNA/RNA extraction kit (QIAGEN). Nucleic acid quantification and quality control were performed using the DNA ScreenTape system (Agilent). A detailed description of WES and RNA-seq data acquisition and analysis are reported in the Supplementary Materials and Methods.

Histological analysis

Formalin-fixed paraffin-embedded 4-μm sections from treatment-naïve endoscopy tumor biopsies of EAC cases diagnosed at San Raffaele Research Hospital between 2014 and 2021 were subjected to IHC. The histological analysis included 30 samples from the prospective EAC patient cohort (ESO-CA001) and 34 from the retrospective cohort (protocols DSAN 718/1F and DSAN 0565/5TF) (Supplementary Figure 1). The primary monoclonal antibodies used for IHC are reported in Supplementary Table 3. Horseradish peroxidase-labeled goat anti-mouse and anti-rabbit IgGs (Zhongshan Golden Bridge Biotechnology, China) were used for IHC as secondary antibodies. Tumor and stromal protein expression was graded with a semi-quantitative h score, ranging from 0 (no staining) to 3 (the strongest staining) based on the prevalence of positive cells. Two histopathologists blinded to the clinical data graded the protein expression.

GeoMX digital spatial profiling

To perform DSP (NanoString, RRID:SCR_021660) on treatment-naïve EAC tissue sections, we first identified tumoral areas based on the morphological analysis of adjacent tissue sections stained with hematoxylin and eosin. Then, on the next tissue section, we performed immunofluorescence staining using customized monoclonal antibodies against pan-cytokeratin (PanCK), hCD3, and hCD68 as morphology markers and a customized multiplexed panel of protein antibodies (n=59). The panel contained photocleavable indexing oligonucleotides, which enabled subsequent readouts.

Spatially non-adjacent regions of interest (ROIs) were selected on a DSP prototype instrument based on immunofluorescent visualization of PanCK (tumor epithelia), CD3 (T lymphocytes), CD68 (macrophages), and DAPI (nuclei). Two custom segmentation masks were generated using PanCK immunofluorescence for separate analysis of $PanCK^+$ (cancer epithelia) and $PanCK^-$ (immune-infiltrated stromal) regions. Ultraviolet light was used to illuminate each segmented ROI, and indexing oligonucleotides were released from each segment. They were then collected and deposited into designated wells on a microtiter plate, allowing for well-indexing of each ROI and direct readout of protein hybridization. For each tissue sample, marker counts were obtained from an average of 4 (range 1–7) PanCK-negative vs. PanCK-positive ROIs. For each marker, raw protein counts per ROI were generated using nCounter45 (nCounter MAX system version 4.0.0.3) and normalized to External RNA Control Consortium controls based on the geometric mean of 3 positive control markers. To measure total protein density, DSP reads were normalized to the ROI area. The DSP analysis suite (Nanostring) was used for

correlation, tSNE, Volcano, and box plots. Statistical analysis of Volcano plots was performed using a linear mixed model.

Flow cytometry

PBMCs or tumor cell suspensions were incubated in PBS with 2% FBS for 15 minutes in Fc Blocker (BD Biosciences, cat. 564220). Afterward, the cells were stained for 20 minutes with mAb panels. To investigate TILs obtained from 6 biopsies, a mAb panel 2 (n=20 mAbs) directed against 20 surface markers (Supplementary Table 4) was used. This panel was used to stain the same TILs that were previously analyzed with the small Treg/Teff panel (CRs n=3, NRs n=3; Supplementary Figure 1). A second independent panel of 10 mAbs, detecting key subset-specific surface markers and 5 intracellular transcription factors associated with specific T cell functions (mAb panel N3, Supplementary Table 4), was used to stain TILs obtained from 6 different baseline EAC biopsies that had not been stained with any previous panel (CRs n=3, NRs n=3; Supplementary Figure 1).

For intracellular/intranuclear staining (panel 3), cells were fixed/permeabilized using the FOXP3/Transcription factor staining kit (eBioscience). The cells were acquired on the BD FACSCanto II (panel 1), BD FACSymphony (panels 2 and 4), or BeckmanCoulter CytoflexLX (panel 3), and analyzed using FlowJo software (Beckton Dickinson, RRID:SCR_008520). Dead cells were identified and excluded by staining with DAPI or using the Live/Dead Fixable Blue Dead Cell Stain Kit (Invitrogen, cat. L23105) upon fixation. The relative fluorescence intensity was calculated from the mean fluorescence intensity (MFI) of the negative control (cluster negative for marker expression) within the corresponding gate. For high-dimensional

analysis, flow cytometry standard data were exported from FlowJo after gating of lymphocytes, singlets, and viable $CD45^+$ cells. The t-distributed stochastic neighbor embedding (t-SNE) maps were built after sample dimensionality reduction to 3000 events, and the PhenoGraph algorithm (https://github.com/jacoblevine/PhenoGraph, RRID:SCR_016919) was applied for cell clustering. The fluorescence intensity of all markers was exported into FlowJo to calculate the cell frequency per cluster and MFI per cluster for each fluorochrome, and samples from CRs and NRs were compared.

Plasma cytokine measurement

To assess 27 cytokines, we used the Bio-Plex Pro-Human 27-plex Assay and followed the manufacturer's instructions. The readouts were obtained using the Bioplex200 machine and Bio-Plex Manager™ 6.0 software (Bio-rad). ELISA was performed using the Complement C3a Human ELISA Kit (Invitrogen, BMS2089), Complement C5a Human ELISA Kit (Invitrogen, BMS2088), and VeriKine-HS Human Interferon Beta Serum ELISA Kit (PBL Assay Science, PBL-41415-1).

Statistical analysis

Statistical analysis was performed using GraphPad Prism 8.0 (GraphPad Software, La Jolla, CA, USA, RRID:SCR_002798). Differences between groups were assessed with two-tailed unpaired t-tests or Wilcoxon tests, unless otherwise specified. Linear correlations between two parameter categories were evaluated using Spearman's rank-order correlation. For multiple group comparisons, the analysis of variance (ANOVA) was performed. A P-value of < 0.05 was considered statistically significant. Overall survival was defined as the time interval between initial surgical excision and death or the last follow-up (censored). Disease survival was defined as the time

interval between initial surgical excision and diagnosis of metastasis/disease progression or the last follow-up. Kaplan–Meier plots were constructed using GraphPad Prism and analyzed using the log-rank test.

Data availability

The data generated in this study are available upon request from the corresponding author. WES and RNAseq data are deposited into the European Genome-phenome Archive (EGA) public repository, accession number EGAS00001007245.

RESULTS

Participants, samples, and study design

To compare the preexisting TME in EAC patients showing variable response to preoperative therapies, we prospectively collected paired blood and endoscopic bioptic tumor samples from patients (n=34) at baseline (i.e., before neoadjuvant therapy) (Figure 1A). Subsequently, the recruited patients underwent nCT alone or in combination with radiotherapy (Supplementary Table 1). All nCT treatment schemes utilized platinum derivative compounds that were mechanistically correlated in terms of their immunomodulatory properties (7, 9). After completing nCT, patients underwent surgery, and the degree of pathological response to treatment was assessed in their resected tumors with the Mandard tumor regression score (TRG) (10). Patients were subdivided into complete responders (CRs, n=12, TRG1-2), partial responders (PRs n=8, TRG3), and non-responders (NRs, n=14, TRG4-5). Although not statistically significant, likely due to the small sample size, CRs showed a better 5-year survival trend compared to PRs and NRs (Supplementary Figure 2A), which was consistent with previous clinical studies (11). Further, the banked baseline

tumor and blood samples collected from this prospective cohort were subjected to a multidimensional analysis, for which different methods were employed depending on sample characteristics (Figure 1A, Supplementary Figure 1). To increase the sample size for IHC and DSP analyses, we added archived clinically annotated baseline EAC biopsies from a second independent retrospective cohort of patients available at San Raffaele Hospital (Supplementary Table 2, Supplementary Figure 1), combining them with the samples from the prospective patient cohort. All findings presented in this report refer to the baseline characteristics of tumors before nCT.

Baseline higher immune gene signatures and reduced resistance to stress are associated with response to neoadjuvant chemotherapy

We performed WES and RNA-seq of 26 baseline EAC samples that passed DNA and RNA quality check; 2 additional EAC samples were subjected to WES only (Supplementary Figure 1). Gene set enrichment analysis (GSEA) of the RNA-seq data revealed significant enrichment of hallmark gene sets related to immune response, type 1 inflammation, and proliferation in CR vs. NR tumors (Figure 1B), suggesting an overall association between nCT response and active immune infiltration, increased cell proliferation, and chemo/chemoradiation vulnerability. EACs of CRs showed significantly higher expression of genes associated with functions consistent with the GSEA pathways, including suppression of tumorigenesis (TRIM71) (12), promotion of T cell receptor signaling and intra-tumor T cell infiltration (CLNK, LCP2/SLP-76) (13, 14), immunoinflammatory response (SLAMF9) (15), suppression of migration (CLEC2L, CARD11, TUSC8) (16, 17), chemotherapy response, and susceptibility to immunogenic cancer cell death ferroptosis (SLC7A11-AS1) (18, 19) (Figure 1C). In contrast, EACs of NRs revealed

significantly enriched pathways associated with resistance to stress, oncogenic activation, peroxisomal function, fatty acid metabolism, and estrogen response (Figure 1B). Notably, the P53 pathway, KRAS signaling downregulated genes, and early estrogen response pathways are known to be associated with the progression of malignant melanoma (20). Baseline EACs of NRs showed significantly higher expression of genes involved in tumor invasion (FGF5, cytokeratin KRT1, and cytokeratin KRT2) (21, 22), oxidative metabolism (SLC13A2, HMGCS2) (23), lipid synthesis (FABP4) (24), and peroxisomal function (PEX16) (25), which is consistent with these hallmarks (Figure 1C). Although EAC cases showing PR to nCT represent a prognostically heterogeneous cohort (residual tumor cells between 10% and 50% in the surgical resection) (10, 26), hallmark GSEA confirmed the upregulation of the same molecular pathways that were differentially expressed in NRs vs. CRs (Supplementary Figure 2B).

We did not observe significant differences in overall TMB, which affects the probability of the formation of tumor neoantigens that TILs may recognize (5). Similarly, no significant differences were seen in tumor neoantigen load between CR and NR tumors (Supplementary Figure 2C-D). This contrasts with the results of previous reports (26), likely due to the smaller sample size of our study (9 CRs vs. 9 NRs). However, compared to CRs and PRs, baseline tumors of NRs exhibited a significantly higher mutational load in genes of the Reactome pathway MHC class I antigen processing and presentation (Figure 1D and Supplementary Figure 2E, Supplementary Table 5). There were no significant differences in mutational load in EAC driver genes (Supplementary Figure 2F-G, Supplementary Table 6). Alterations in the presentation of MHC class I antigens are associated with a worse prognosis of

several malignancies (27) and may negatively impact the anti-tumor immune response in EAC. In our sample, only 1 NR and 1 PR case demonstrated loss of heterozygosity of HLA class I alleles (Figure 1E), another factor correlated with reduced likelihood of MHC class I antigen presentation (28).

Collectively, these results suggest that response to nCT was dependent on pre-existing active immune infiltration and higher susceptibility to chemotherapy and radiotherapy in the responding tumors. On the other hand, non-responding tumors were characterized by increased immunosuppression and resistance to oxidative stress.

Distinct baseline patterns of myelomonocytic and T cell infiltration distinguish responders from non-responders to neoadjuvant chemotherapy

To better understand the differences in immune contextures between CRs and NRs, as suggested by the genomic analysis, we used the Cibersort tool to estimate the immune composition of the tumor biopsies from bulk RNA-seq data. Our analysis revealed significantly reduced signatures for immunosuppressive T regulatory cells (Tregs) and M2-like macrophages in CRs compared to NRs (Figure 2A).

We then performed IHC of specific immune cell markers to confirm the differential tumor infiltration of immunosuppressive Tregs and M2-like macrophages between CRs and NRs and subsequently examine potential anti-tumor effector T cells. We stained sections of 30 prospectively collected baseline EAC biopsies with markers for Treg (Foxp3), M2-like macrophage (CD163), and effector memory T cells (CD45RO) (Figure 2B). The results showed that NRs exhibited a trend toward increased peritumoral FoxP3 and CD163 staining, while CRs showed higher levels

of intra-tumoral CD45RO staining (Supplementary Figure 3A). To validate these findings, we stained baseline EAC biopsies from an independent retrospective archived cohort (n = 34 cases) and confirmed significantly higher levels of staining for CD163 in NRs compared to CRs (Supplementary Figure 3B). We also confirmed the trend for increased Foxp3 and decreased CD45RO in baseline EAC biopsies. By combining data from the two cohorts, we further confirmed higher levels of "immunoregulatory" Foxp3 and CD163 expression in NRs compared to CRs, which was statistically significant (Figure 2C). Additionally, we observed higher levels of CD45RO in CRs, indicating enrichment for intra-tumoral effector memory cells (Figure 2C). Moreover, a trend for higher peritumoral staining scores for Foxp3 and CD163 and for lower intra-tumoral staining scores for CD45RO was still present in each separate group of NRs who received either combined nCT and radiotherapy (nCT+RT) or neoadjuvant chemotherapy alone (nCT), indicating a common underlying immune mechanism associated with treatment response to both neoadjuvant regimens (Supplementary Figure 3C-D). No significant differences in the levels of CD3, CD4, CD8, or the pan-macrophage marker CD68 were detected (Supplementary Figure 4A-B). Remarkably, higher levels (h≥2) of peri-tumoral Foxp3 staining and CD163 immunostaining were associated with reduced overall survival in the two combined cohorts of EAC patients (Figure 2D-F).

Digital spatial profiling supports differential baseline tumor immune infiltration in complete responders and non-responders

To enhance the tissue analysis with spatial resolution information, we conducted multiplex proteomic analysis using DSP on baseline EACs. Tumor sections were stained with 53 mAbs to detect functional immune markers or proteins involved in

known cell functions, followed by the analysis of selected ROIs (Figure 3A). DSP for 53 tumor and immune proteins was performed on 144 regions of tumor sections obtained from 2–4 pooled EAC biopsies for each of the CR (n=9) and NR (n=10) tumors. Spatially separated ROIs were selected by visualizing the markers PanCK (tumor epithelia), CD3 (T lymphocytes), CD68 (macrophages), and DAPI (nuclei) using immunofluorescence. $PanCK^+$ cancer epithelial regions were compared with $PanCK^-$ immune-infiltrated stromal regions (Figure 3A-B; Supplementary Figure 5A-F). We found significantly higher expression of the epithelial markers PanCK and EpCAM in $PanCK^+$ cancer cell areas, in contrast to the increased expression of the stromal markers alpha smooth muscle actin (SMA) and fibronectin and the lymphocytic markers CD3 and CD39 in $PanCK^-$ stromal regions (Figure 3B). The ratios of the CD3 signal in $PanCK^+$ areas to the CD3 signal in $PanCK^-$ areas were significantly higher in the ROIs of CRs compared to NRs (Figure 3C-D). This finding suggests a higher frequency of tumor-infiltrating T cells in EACs of CRs, indicating a possible correlation with the anti-tumoral immune response. Furthermore, $PanCK^-$ areas showed enrichment for Foxp3 and CD163 protein expression in NRs, indicating significantly increased infiltration by immunosuppressive Tregs and M2-like macrophages, which was consistent with our IHC data. The immune checkpoint molecule TIM3 and inflammation-related signaling mediator stimulator of interferon genes (STING) were also enriched in NRs (Figure 3E-F). In addition, within the $PanCK^+$ cancer cell areas of NR tumors, there were significantly elevated levels of the anti-apoptotic protein Bcl-2 (associated with tumor survival; 29), alpha SMA (associated with invasion and metastasis in gastric cancer; 30), and the estrogen receptor alpha and progesterone receptor (correlated with prognosis of EAC and gastric cancer; 31, 32) (Figure 3G-H).

Together, the spatially resolved tissue proteomics results provided additional evidence to support the characterization of a highly immunoreactive tumor infiltrate in baseline tumors of CRs, in contrast to an actively immunosuppressive and therapy-resistant infiltrate in tumors of NRs. This analysis also highlighted additional protein markers associated with the absence of a pathological response to nCT that could be further explored as potential therapeutic targets.

Distinct myelomonocytic and T cell populations in baseline tumors of complete responders versus non-responders to neoadjuvant chemotherapy

To examine the differentially infiltrating EAC immune populations in greater detail, we used flow cytometry to characterize TILs from 15 baseline tumor biopsies in the prospective cohort (Supplementary Figure 1) using a panel of 7 mAbs detecting Treg and effector T cells (mAb panel N1, Supplementary Table 4). This analysis confirmed the significant enrichment of cells expressing a putative Treg phenotype in NR tumors ($CD25^{+}CD127^{low}CD4^{+}$) (Figure 4A-B), whereas CR tumors were characterized by a higher frequency of tissue-resident memory $CD39^{+}CD103^{+}CD8^{+}$ T cells (Figure 4A,C), a population of cells often enriched in other solid tumors (33). We further deep-profiled the functional phenotype of TILs in baseline EAC biopsies using high-dimensional flow cytometry with two complementary mAb panels (panels N2 and N3, Supplementary Table 4, Supplementary Figure 6A-C). In NRs, unsupervised high-dimensional analysis of $CD4^{+}$ TILs highlighted a significantly increased frequency of putative $CD25^{+}CD127^{low}CD39^{+}PD1^{+}TIM3^{+}$ Treg cells found in two clusters (#4 and #5; Figure 4D-E, Supplementary Figure 7A,C), differentiated by the expression of KLRG1. The increased frequency of $TIM3^{+}$ Tregs in TILs of NRs was consistent with the previous DSP data, which showed higher levels of TIM3

protein in baseline tumor biopsies of NRs. Additionally, a third cluster of $CD4^+$ TILs (#9) containing putative exhausted $CD39^+LAG3^+CD28^-$ T effector memory cells (Supplementary Figure 7A,C) showed their preferential accumulation in NRs. Furthermore, unsupervised clustering analysis of $CD8^+$ TILs in NRs revealed a highly enriched cluster (#2) displaying a $CD103^-CD69^-CD45RO^-CCR7^-CD28^-KLRG1^+LAG3^+$ phenotype, highly suggestive of exhausted and terminally differentiated non-tissue-resident effector cells (Figure 4F-G, Supplementary Figure 8A,C). In contrast, CRs were characterized by an enriched population (#1) of tissue-resident memory $CD45RO^+CD39^+CD103^+CD69^+CCR7^-$ T cells that co-expressed CD28, CXCR5, and the exhaustion marker PD-1, but were negative for CD127 and all tested inhibitory receptors (Figure 4F,G, Supplementary Figure 8A,C). This population of cells is similar to an early dysfunctional tissue-resident $CXCR5^+CD8^+$T cell subset that sustains effector responses in different cancers and chronic viral infections, and that is positively associated with response to anti-PD-1 immunotherapy (34, 35). The flow cytometric assessment of nuclear transcription factors expressed in $CD4^+$ T cells confirmed the accumulation of $CD25^{high}CD127^{low}Foxp3^+$ Tregs (#6) in tumors of NRs, with no significant differences in the expression of other transcription factors (Figure 4H-I, Supplementary Figure 7B,D). The analysis of nuclear transcription factors expressed in putative $CD8^+$effector/memory TILs ($CD45RO^+CD4^-$ cells) showed an increased frequency of T-$bet^{high}EOMES^+$ cells (subset #3) in CRs (Figure 4J-K, Supplementary Figure 8B,D), reminiscent of early exhausted tumor-infiltrating cells found to sustain anti-tumor or chronic anti-viral responses (35).

The myeloid cell composition of baseline tumor biopsies was also characterized by high-dimensional flow cytometric analysis of 22 extracellular markers (mAb panel N4, Supplementary Table 4, Supplementary Figure 9). Unsupervised cluster analysis of the myeloid cell staining identified 10 populations (Figure 5A), with only M2-like macrophages (#3, $CD14^{+}CD163^{+}ICAM\text{-}1^{+}HLA\text{-}DR^{hi}CD33^{-}$) being significantly more frequent in NR tumors than in CR tumors (Figure 5 B,C, Supplementary Figure 10), which further corroborated the results of our histological analysis.

Collectively, these results suggest that CR tumors have a pre-existing immunoreactive contexture characterized by enrichment for tissue-resident, putatively tumor-reacting, early exhausted $CD8^{+}$ TILs. In contrast, an immunosuppressive contexture characterized by enrichment for Treg and M2-like tumor-associated macrophages (TAM) was identified in baseline NR tumors.

Differences in baseline circulating T and myeloid cell populations and soluble immune mediators distinguish complete responders and non-responders

In addition to analyzing the local immune TME, we also evaluated systemic immune markers associated with response to nCT in baseline PBMCs obtained from 16 EAC patients in our prospective cohort. We used high-dimensional flow cytometry with 20 and 22 mAbs panels (panels N2 and N4, Supplementary Table 4) to assess T cell and myelomonocytic phenotypes, respectively (Supplementary Figure 1). Unsupervised clustering analysis of T lymphocytes was performed separately for $CD4^{+}$ and $CD8^{+}$ T cells (Supplementary Figure 11A-B and 12A-B), which revealed an increased frequency of exhausted $KLRG1^{high}PD1^{high}CD4^{+}$ effector memory cells (#6, Figure 6A-B, Supplementary Figure 11B) and $TIGIT^{high}PD1^{high}CD8^{+}$ transitional

memory cells (#8, Figure 6C,D, Supplementary Figure 12B) in NR tumors. We also performed the unsupervised clustering analysis of 20 extracellular markers expressed by $CD45^{+}CD3^{-}$ circulating immune cells and identified 11 distinct populations (Figure 6E, Supplementary Figure 13). In the pre-treatment blood of NRs, there was a significant enrichment of monocytic myeloid-derived suppressor cells (MO-MDSCs, cluster #4) expressing PD-L1 and CCR7 compared to CRs (Figure 6E-G), suggesting that this population may suppress the anti-tumoral immune response and negatively affect the efficacy of nCT (36). Conversely, the pre-treatment blood of CRs showed a higher frequency of putative inflammatory $CD14^{+}CD11c^{+}HLA\text{-}DR^{high}$ monocyte cluster (#1), indicating a potentially increased pool of immunostimulatory cells capable of infiltrating the tumor upon therapy (Figure 6E-G). Notably, the frequency of this putative circulating inflammatory monocyte population was positively correlated with the frequency of putative tumor-reactive $CD39^{+}CD103^{+}CD8^{+}$ TILs, which characterizes baseline tumors in CRs (Figure 6H).

Finally, we performed a comparison of the plasma concentration of 30 cytokines and chemokines in baseline blood samples from 26 patients of the prospective cohort (Figure 7, Supplementary Figure 1, Supplementary Figure 14). Our analysis found that the plasma of CRs had higher concentrations of GM-CSF, a cytokine that positively affects the anti-tumor T lymphocyte response (37) (Figure 7A), whereas the plasma of NRs contained a significantly higher concentration of IL-4, CXCL10, C3a, and C5a (Figure 7A), the immune effectors associated with immunosuppression by MO-MDSCs (38-40). The frequency of putative anti-tumor $CD8^{+}CD39^{+}CD103^{+}$ TILs was positively correlated with the plasma concentration of GM-CSF, RANTES, and IL1RA, but was negatively correlated with IL-4

concentration (Figure 7B,C). In addition, the baseline frequency of the circulating putative inflammatory $CD14^{+}CD11c^{+}HLA\text{-}DR^{high}$ monocyte population was positively correlated with the baseline plasma concentration of GM-CSF (Figure 7D). These results indicate that differential baseline immune determinants of response to nCT were also detectable in EAC patients at the systemic level and were correlated with intra-tumor and systemic cellular immune parameters.

DISCUSSION

In this study, we provide evidence that the pre-existing immunity within baseline tumor tissues drives the clinical effects of nCT among patients with locally advanced EAC. These results strongly suggest that the immune composition of the TME prior to treatment impacts the outcomes of nCT.

Our study analyzed genomic data from baseline EAC biopsies and revealed that patients who showed a complete response to nCT had higher expression of immune response genes within their tumors. Our findings suggest that a functional MHC class I antigen presentation pathway is necessary to achieve a therapeutic response. Previous studies have linked a deficiency in the DNA damage and immune response (DDIR) pathway (41) and a higher non-synonymous TMB (26) with a better response to nCT in EAC. Although we did not detect baseline DDIR signatures or higher TMB in our cohort of EAC responders to nCT, possibly due to the smaller sample size relative to previous studies (26, 41), the identified associations between immune-related pathways and response to nCT are mechanistically consistent with those studies.

Recent research has demonstrated an association between nCT response, baseline T cell infiltration, and $CD8^+PD1^+$ staining scores in EAC (42, 43). Here, we utilized multiple approaches to gain a more comprehensive understanding of the immune landscape in baseline tumors, which was associated with a positive or negative therapeutic response to nCT at both local and systemic levels. Our findings revealed that CR tumors had a high frequency of tissue-resident memory $CD39^+PD1^+CD8^+$ TILs, a population highly enriched for tumor antigen specificity and present in other solid tumors (33). Furthermore, we observed a high frequency of effector/memory $CD8^+$ TILs expressing T-bet and EOMES in CR tumors. This combination of transcription factors is characteristic of early exhausted TILs, which are capable of sustaining anti-tumor or chronic anti-viral responses (34, 35). In contrast, our findings indicated that NR tumors had a predominantly suppressive immune contexture characterized by a high frequency of Treg cells and $CD163^+$ M2-like TAMs, both of which are associated with reduced overall patient survival. These results were consistent with recent reports (42), We also observed a higher frequency of circulating immunostimulatory $CD14^+CD11c^+$HLA-DR^{high} monocytes in CRs, whereas NRs showed a higher frequency of circulating immunosuppressive $CCR7^+PDL1^+$ MO-MDSCs.

Using spatially resolved proteomic analysis of treatment-naïve EACs, we confirmed higher baseline levels of CD163 and Foxp3 in the tumor infiltrate of NR samples. Additionally, the analysis revealed higher expression of the immune checkpoint inhibitor TIM3, which is expressed by Treg cells, enhancing the immunosuppressive function in cancer (44). Thus, in our study, increased levels of TIM3 were likely attributed to the higher frequency of Tregs seen in NRs, although the expression of

TIM3 by other tumor-infiltrating immune populations cannot be completely ruled out. The DSP analysis also revealed significantly higher expression of STING in the immune-infiltrated stromal regions of NR tumors. Although STING induces anti-cancer IFN type I signaling, its activation in T cells may also prevent proliferation, promote cell death, and activate immune suppressive cells under certain conditions (45).

We also detected systemic differences in the blood samples of CRs vs. NRs prior to treatment. Specifically, NRs had higher baseline plasma concentrations of suppressive cytokines CXCL10 and IL-4, both of which may affect the migration and function of MDSCs (38, 39). Furthermore, NRs had significantly higher pre-nCT plasma concentrations of complement anaphylatoxins C3a and C5a, which mediate the migration of suppressive immune cell populations within tumors and tumor-draining lymph nodes (40).

In addition to detecting distinct immune profiles, our multidimensional analysis revealed specific cancer cell-intrinsic differences between CRs and NRs. Specifically, baseline gene signatures were associated with cell cycle control in CRs, suggesting that the proliferative ability of cancer cells may impact treatment response to nCT. Similar pathways have also been shown to predict nCT responsiveness in ER-positive/HER2-negative breast cancer patients (46), although the underlying mechanisms are not fully understood. On the other hand, NR tumors were characterized by gene signatures correlated with lipid metabolism and peroxisomes, pathways associated with cancer resistance to chemo/radiation-induced damage and tumorigenesis (24, 47). The enrichment of a lipid metabolism

genetic signature may be related not only to the metabolic requirements of the tumor but also to the functional profile of immune cells within the TME (48), which warrants further investigation. For instance, the activity of immune suppressive cells such as Tregs and M2-like macrophages depends on fatty acid oxidation (49). Moreover, heightened lipid uptake and β-oxidation are characteristic of a hypoglycemic TME that is associated with poor tumor antigen presentation (50). Dysregulated cholesterol accumulation in the TME has also been linked to the induction of immunosuppressive cues (51), which is consistent with the suppressive immune contexture observed in EACs of NRs. These metabolic signatures represent potential vulnerabilities of cancer cells that could be targeted to reverse EAC resistance to nCT. In fact, several drugs are currently being investigated for targeting lipid metabolism in solid malignancies, such as gastric cancer (47), that could be combined with current nCT to improve their success rate.

Furthermore, our transcriptional analysis revealed significant enrichment of the long non-coding RNA SLC7A11-AS1 expression in CR tumors prior to nCT treatment. Previous studies have reported that SLC7A11-AS1 expression is correlated with the chemotherapy response in gastric cancer and, interestingly, with the suppression of SLC7A11 gene expression (18). SLC7A11 is an antioxidant cystine/glutamate antiporter implicated in the inhibition of ferroptosis, an immunogenic cancer cell death induced by radiotherapy and the anti-tumor CD8 T-cell IFNγ response (19). Although further validation is needed, our findings hint at the fact that EAC cells may be resistant to nCT due to the inhibition of ferroptosis, which could potentially be targeted by certain drugs (19). Moreover, our DSP data revealed increased expression of the anti-apoptotic protein Bcl-2 and the stromal protein alpha SMA in

cancer cells of NRs, suggesting increased baseline tumor resistance to apoptosis and its metastatic potential (29, 30). Additionally, increased expression of alpha estrogen and progesterone receptors was observed in NR tumors, which could potentially be validated as markers of resistance to nCT and plausible therapeutic targets in future research.

The expression data obtained from NR tumors also revealed TIM3 as a potential candidate target for immune checkpoint blockade therapy. TIM3 is expressed by a variety of cell types, including Tregs, and its function is not solely attributed to immune suppression (44). Available clinical data have shown that blocking TIM-3 in advanced treatment-refractory solid tumors, either alone or in combination with PD-1 or PD-L1 blockade, has only had modest anti-tumor activity (52). However, EAC was not included in these studies, and our data suggest that targeting TIM-3 in this malignancy, either alone or in combination with PD-1 blockade and/or chemo/chemoradiotherapy (44), may represent a viable therapeutic option. Although our results are consistent with a model of nCT according to which it stimulates the pre-existing spontaneous anti-tumor T cell response, these treatments may also induce the anti-tumor T cell response de novo. Indeed, clinical trials have demonstrated that some EAC patients who did not respond to nCT showed positive response to adjuvant anti-PD1 immunotherapy (53). Thus, exploring novel approaches for combining immunotherapies with chemotherapy, with or without radiotherapy, represents a promising avenue for further investigation (54). Validation of robust biomarkers will facilitate the identification of optimal patient candidates for receiving combination regimens. Notably, we observed a positive correlation between baseline infiltration of putative tumor-reactive $CD39^{+}CD103^{+}CD8^{+}$ TILs and

circulating inflammatory HLA-DR^{high} monocytes in CRs. Furthermore, CD39^{+}CD103^{+}CD8^{+} TILs showed a positive correlation with pre-treatment circulating levels of the pro-inflammatory cytokines GM-CSF, IL1RA, and RANTES, and a negative correlation with IL-4 concentration in the plasma. The detection of circulating MDSCs may also help distinguish CRs from NRs. Taken together, these systemic cellular and biochemical markers may represent a proxy for active tumor immune T cell infiltration to serve as a predictor of response to nCT.

We acknowledge that the small number of patients included in our study is a limitation. However, the deep and comprehensive multidimensional analysis performed on paired tumor and blood samples from the same patients mitigates this limitation, as it possibly serves as one of the largest in-depth analyses of baseline EAC samples from a prospective cohort of patients. The results reported in this study are exploratory and hypothesis-generating, and rigorous validation in larger cohorts is needed. Moreover, the patients included in this study underwent two standard-of-care therapies for EAC, nCT alone or in combination with radiotherapy, both of which use platinum derivatives that have stimulatory effects on the anti-tumor immune response by either promoting immunogenic forms of cancer cell death or directly activating immune effector cells (7-9). Indeed, our baseline intra-tumor and systemic immune signatures, which predispose patients to respond to nCT, were consistent across both regimens, suggesting a shared mechanistic background between the two.

In conclusion, our study identifies novel potential immune markers and molecular pathways associated with therapeutic response or resistance to nCT in EAC. Further

validation of these markers and pathways is needed to improve the prediction of response to nCT and guide the development of personalized therapeutic options.

ACKNOWLEDGEMENTS

The authors thank the staff of the Gastrointestinal Surgery Unit at San Raffaele Hospital for their support in patient enrollment and clinical sample collection, the staff of the Center for OMICs Sciences at San Raffaele Institute for their feedback on the sample processing and the analysis of next-generation sequencing data, Drs. Claudia De Lalla and Cristina Faccani from the Experimental Immunology Unit at San Raffaele Institute for their feedback on the analysis of high-dimensional flow cytometry data, and the patients participating to the ESOCA-001, DSAN 718/1F and DSAN 0565/5TF studies.

FUNDING

This study was supported by the European Molecular Biology Organization grant ALTF 1358-2016, European Commission Marie Curie Individual Fellowship Grant IC_IL_EC_2017, L'Oréal UNESCO for Women in Science Italy, and Italian Association For Cancer Research Grant MFAG 24780.

COMPETING INTERESTS

None declared.

REFERENCES

1. Smyth EC, Lagergren J, Fitzgerald RC, Lordick F, Shah MA, Lagergren P, Cunningham D. Oesophageal cancer. Nat Rev Dis Primers. 2017;3:17048.

2. Shapiro J, van Lanschot JJB, Hulshof M, van Hagen P, van Berge Henegouwen MI, Wijnhoven BPL, van Laarhoven HWM, Nieuwenhuijzen GAP, Hospers GAP, Bonenkamp JJ, Cuesta MA, Blaisse RJB, Busch ORC, Ten Kate FJW, Creemers GM, Punt CJA, Plukker JTM, Verheul HMW, Bilgen EJS, van Dekken H, van der Sangen MJC, Rozema T, Biermann K, Beukema JC, Piet AHM, van Rij CM, Reinders JG, Tilanus HW, Steyerberg EW, van der Gaast A; CROSS study group. Neoadjuvant chemoradiotherapy plus surgery versus surgery alone for oesophageal or junctional cancer (CROSS): long-term results of a randomised controlled trial. Lancet Oncol. 2015;16:1090-8.

3. Obermannová R, Alsina M, Cervantes A, Leong T, Lordick F, Nilsson M, van Grieken NCT, Vogel A, Smyth EC; ESMO Guidelines Committee. Oesophageal cancer: ESMO Clinical Practice Guideline for diagnosis, treatment and follow-up. Ann Oncol. 2022 Oct;33(10):992-1004.

4. Fridman WH, Pagès F, Sautès-Fridman C, Galon J. The immune contexture in human tumours: impact on clinical outcome. Nature Reviews Cancer. 2012;12:298-306.

5. Mennonna D, Maccalli C, Romano MC, Garavaglia C, Capocefalo F, Bordoni R, Severgnini M, De Bellis G, Sidney J, Sette A, Gori A, Longhi R, Braga M, Ghirardelli L, Baldari L, Orsenigo E, Albarello L, Zino E, Fleischhauer K, Mazzola G, Ferrero N, Amoroso A, Casorati G, Parmiani G, Dellabona P. T cell neoepitope discovery in colorectal cancer by high throughput profiling of somatic mutations in expressed genes. Gut. 2017 Mar;66(3):454-463.

6. Ribas A, Wolchok JD. Cancer immunotherapy using checkpoint blockade. Science. 2018;359:1350-5.

7. Galluzzi L, Senovilla L, Zitvogel L, Kroemer G. The secret ally: immunostimulation by anticancer drugs. Nat Rev Drug Discov. 2012 Feb 3;11(3):215-33.

8. Lhuillier C, Rudqvist NP, Elemento O, Formenti SC, Demaria S. Radiation therapy and anti-tumor immunity: exposing immunogenic mutations to the immune system. Genome Med. 2019;11:40.

9. Kroemer G, Galassi C, Zitvogel L, Galluzzi L. Immunogenic cell stress and death. Nat Immunol. 2022 Apr;23(4):487-500.

10. Mandard AM, Dalibard F, Mandard JC, Marnay J, Henry-Amar M, Petiot JF, Roussel A, Jacob JH, Segol P, Samama G, Ollivier JM, Bonvalot S., Gignoux M. Pathologic assessment of tumor regression after preoperative chemoradiotherapy of esophageal carcinoma. Clinicopathologic correlations. Cancer. 1994 Jun 1;73(11):2680-6.

11. Donahue JM, Nichols FC, Li Z, Schomas DA, Allen MS, Cassivi SD, Jatoi A, Miller RC, Wigle DA, Shen KR, Deschamps C. Complete pathologic response after neoadjuvant chemoradiotherapy for esophageal cancer is associated with enhanced survival. Ann Thorac Surg. 2009 Feb;87(2):392-8; discussion 398-9.

12. Chen Y, Hao Q, Wang J, Li J, Huang C, Zhang Y, Wu X, Lu H, Zhou X. Ubiquitin ligase TRIM71 suppresses ovarian tumorigenesis by degrading mutant p53. Cell Death Dis. 2019 Sep 30;10(10):737.

13. Jordan MS, Koretzky GA. Coordination of receptor signaling in multiple hematopoietic cell lineages by the adaptor protein SLP-76. Cold Spring Harb Perspect Biol. 2010 Apr;2(4):a002501.

14. Wang Z, Peng M. A novel prognostic biomarker LCP2 correlates with metastatic melanoma-infiltrating CD8+ T cells. Sci Rep. 2021 Apr 28;11(1):9164.

15. Dollt C, Michel J, Kloss L, Melchers S, Schledzewski K, Becker K, Sauer A, Krewer A, Koll F, Schmieder A. The novel immunoglobulin super family receptor SLAMF9 identified in TAM of murine and human melanoma influences pro-inflammatory cytokine secretion and migration. Cell Death Dis. 2018 Sep 19;9(10):939.

16. Wang L, Yin J, Wang X, Shao M, Duan F, Wu W, Peng P, Jin J, Tang Y, Ruan Y, Sun Y, Gu J. C-Type Lectin-Like Receptor 2 Suppresses AKT Signaling and Invasive Activities of Gastric Cancer Cells by Blocking Expression of Phosphoinositide 3-Kinase Subunits. Gastroenterology. 2016 May;150(5):1183-1195.e16.

17. Hu R, Bi R, Jiang L, Yang X, Zhong Y, Xie X. LncRNA TUSC8 suppresses the proliferation and migration of esophageal cancer cells by downregulation of VEGFA. J Cancer. 2021 Sep 3;12(21):6393-6400.

18. Luo Y, Xiang W, Liu Z, Yao L, Tang L, Tan W, Ye P, Deng J, Xiao J. Functional role of the SLC7A11-AS1/xCT axis in the development of gastric cancer cisplatin-resistance by a GSH-dependent mechanism. Free Radic Biol Med. 2022 May 1;184:53-65.

19. Lang X, Green MD, Wang W, Yu J, Choi JE, Jiang L, Liao P, Zhou J, Zhang Q, Dow A, Saripalli AL, Kryczek I, Wei S, Szeliga W, Vatan L, Stone EM, Georgiou G, Cieslik M, Wahl DR, Morgan MA, Chinnaiyan AM, Lawrence TS, Zou W. Radiotherapy and Immunotherapy Promote Tumoral Lipid Oxidation and Ferroptosis via Synergistic Repression of SLC7A11. Cancer Discov. 2019 Dec;9(12):1673-1685.

20. Han W, Hu C, Fan ZJ, Shen GL. Transcript levels of keratin 1/5/6/14/15/16/17 as potential prognostic indicators in melanoma patients. Sci Rep. 2021 Jan 13;11(1):1023.

21. Iwabu J, Yamashita S, Takeshima H, Kishino T, Takahashi T, Oda I, Koyanagi K, Igaki H, Tachimori Y, Daiko H, Nakazato H, Nishiyama K, Lee YC, Hanazaki K, Ushijima T. FGF5 methylation is a sensitivity marker of esophageal squamous cell carcinoma to definitive chemoradiotherapy. Sci Rep. 2019 Sep 16;9(1):13347.

22. Toivola DM, Boor P, Alam C, Strnad P. Keratins in health and disease. Curr Opin Cell Biol. 2015 Feb;32:73-81.

23. Lee YE, He HL, Shiue YL, Lee SW, Lin LC, Wu TF, Chang IW, Lee HH, Li CF. The prognostic impact of lipid biosynthesis-associated markers, HSD17B2 and HMGCS2, in rectal cancer treated with neoadjuvant concurrent chemoradiotherapy. Tumour Biol. 2015 Sep;36(10):7675-83.

24. Luis G, Godfroid A, Nishiumi S, Cimino J, Blacher S, Maquoi E, Wery C, Collignon A, Longuespée R, Montero-Ruiz L, Dassoul I, Maloujahmoum N, Pottier C, Mazzucchelli G, Depauw E, Bellahcène A, Yoshida M, Noel A, Sounni NE. Tumor resistance to ferroptosis driven by Stearoyl-CoA Desaturase-1 (SCD1) in cancer cells and Fatty Acid Biding Protein-4 (FABP4) in tumor microenvironment promote tumor recurrence. Redox Biol. 2021 Jul;43:102006.

25. Dahabieh MS, Di Pietro E, Jangal M, Goncalves C, Witcher M, Braverman NE, Del Rincón SV. Peroxisomes and cancer: The role of a metabolic specialist in a disease of aberrant metabolism. Biochim Biophys Acta Rev Cancer. 2018 Aug;1870(1):103-121.

26. Izadi F, Sharpe BP, Breininger SP, Secrier M, Gibson J, Walker RC, Rahman S, Devonshire G, Lloyd MA, Walters ZS, Fitzgerald RC, Rose-Zerilli MJJ, Underwood

TJ, On Behalf Of Occams. Genomic Analysis of Response to Neoadjuvant Chemotherapy in Esophageal Adenocarcinoma. Cancers (Basel). 2021 Jul 6;13(14):3394.

27. Dhatchinamoorthy K, Colbert JD, and Kenneth L. Rock KL. Cancer Immune Evasion Through Loss of MHC Class I Antigen Presentation. Front Immunol. 2021; 12: 636568.

28. McGranahan N, Rosenthal R, Hiley CT, Rowan AJ, Watkins TBK, Wilson GA, Birkbak NJ, Veeriah S, Van Loo P, Herrero J, Swanton C; TRACERx Consortium. Allele-Specific HLA Loss and Immune Escape in Lung Cancer Evolution. Cell. 2017 Nov 30;171(6):1259-1271.e11.

29. Cory S, Huang DC, Adams JM. The Bcl-2 family: roles in cell survival and oncogenesis. Oncogene. 2003 Nov 24;22(53):8590-607.

30. Pearce OMT, Delaine-Smith RM, Maniati E, Nichols S, Wang J, Böhm S, Rajeeve V, Ullah D, Chakravarty P, Jones RR, Montfort A, Dowe T, Gribben J, Jones JL, Kocher HM, Serody JS, Vincent BG, Connelly J, Brenton JD, Chelala C, Cutillas PR, Lockley M, Bessant C, Knight MM, Balkwill FR. Deconstruction of a Metastatic Tumor Microenvironment Reveals a Common Matrix Response in Human Cancers. Cancer Discov. 2018 Mar;8(3):304-319.

31. Al-Khyatt W, Tufarelli C, Khan R, Iftikhar SY. Selective oestrogen receptor antagonists inhibit oesophageal cancer cell proliferation in vitro. BMC Cancer. 2018 Feb 1;18(1):121.

32. Li M, Zhou C. Progesterone receptor gene serves as a prognostic biomarker associated with immune infiltration in gastric cancer: a bioinformatics analysis. Transl Cancer Res. 2021 Jun;10(6):2663-2677.

33. Duhen T, Duhen R, Montler R, Moses J, Moudgil T, de Miranda NF, Goodall CP, Blair TC, Fox BA, McDermott JE, Chang SC, Grunkemeier G, Leidner R, Bell RB, Weinberg AD. Co-expression of CD39 and CD103 identifies tumor-reactive CD8 T cells in human solid tumors. Nat Commun. 2018 Jul 13;9(1):2724.

34. Losurdo A, Scirgolea C, Alvisi G, Brummelman J, Errico V, Di Tommaso L, Pilipow K, Colombo FS, Fernandes B, Peano C, Testori A, Tinterri C, Roncalli M, Santoro A, Mazza EMC, Lugli E. Single-cell profiling defines the prognostic benefit of CD39high tissue resident memory CD8+ T cells in luminal-like breast cancer. Commun Biol. 2021 Sep 22;4(1):1117.

35. McLane LM, Abdel-Hakeem MS, Wherry EJ. CD8 T Cell Exhaustion During Chronic Viral Infection and Cancer. Annu Rev Immunol. 2019 Apr 26;37:457-495.

36. Shields JD, Kourtis IC, Tomei AA, Roberts JM, Swartz MA. Induction of lymphoidlike stroma and immune escape by tumors that express the chemokine CCL21. Science. 2010 May 7;328(5979):749-52.

37. Zarei S, Schwenter F, Luy P, Aurrand-Lions M, Morel P, Kopf M, Dranoff G, Mach N. Role of GM-CSF signaling in cell-based tumor immunization. Blood. 2009 Jun 25;113(26):6658-68.

38. Mandruzzato S, Solito S, Falisi E, Francescato S, Chiarion-Sileni V, Mocellin S, Zanon A, Rossi CR, Nitti D, Bronte V, Zanovello P. IL4Ralpha+ myeloid-derived suppressor cell expansion in cancer patients. J Immunol. 2009 May 15;182(10):6562-8.

39. Liu H, Ling CC, Yeung WHO, Pang L, Liu J, Zhou J, Zhang WY, Liu XB, Ng TPK, Yang XX, Lo CM, Man K. Monocytic MDSC mobilization promotes tumor recurrence after liver transplantation via CXCL10/TLR4/MMP14 signaling. Cell Death Dis. 2021 May 14;12(5):489

40. Llaudo I, Fribourg M, Medof ME, Conde P, Ochando J, Heeger PS. C5aR1 regulates migration of suppressive myeloid cells required for costimulatory blockade-induced murine allograft survival. Am J Transplant. 2019 Mar;19(3):633-645.

41. Turkington RC, Knight LA, Blayney JK, Secrier M, Douglas R, Parkes EE, Sutton EK, Stevenson L, McManus D, Halliday S, McCavigan AM, Logan GE, Walker SM, Steele CJ, Perner J, Bornschein J, MacRae S, Miremadi A, McCarron E, McQuaid S, Arthur K, James JA, Eatock MM, O'Neill R, Noble F, Underwood TJ, Harkin DP, Salto-Tellez M, Fitzgerald RC, Kennedy RD; Oesophageal Cancer Clinical and Molecular Stratification (OCCAMS) Study Group. Immune activation by DNA damage predicts response to chemotherapy and survival in oesophageal adenocarcinoma. Gut. 2019 Nov;68(11):1918-1927.

42. Goedegebuure RSA, Harrasser M, de Klerk LK, van Schooten TS, van Grieken NCT, Eken M, Grifhorst MS, Pocorni N, Jordanova ES, van Berge Henegouwen MI, Pouw RE, Verheul HMW, van der Vliet JJ, van Laarhoven HWM, Thijssen VLJL, Bass AJ, De Gruijl TD, Derks S. Pre-treatment tumor-infiltrating T cells influence response to neoadjuvant chemoradiotherapy in esophageal adenocarcinoma. Oncoimmunology. 2021 Aug 4;10(1):1954807.

43. Soeratram TT, Creemers A, Meijer SL, de Boer OJ, Vos W, Hooijer GK, van Berge Henegouwen MI, Hulshof MC, Bergman JJ, Lei M, Bijlsma MF, Ylstra B, van Grieken NC, van Laarhoven HW. Tumor-immune landscape patterns before and after chemoradiation in resectable esophageal adenocarcinomas. J Pathol. 2022 Mar;256(3):282-296.

44. Tian T, Li Z. Targeting Tim-3 in Cancer With Resistance to PD-1/PD-L1 Blockade. Front Oncol. 2021 Sep 22;11:731175.

45. Cerboni S, Jeremiah N, Gentili M, Gehrmann U, Conrad C, Stolzenberg MC, Picard C, Neven B, Fischer A, Amigorena S, Rieux-Laucat F, Manel N. Intrinsic antiproliferative activity of the innate sensor STING in T lymphocytes. J Exp Med. 2017;214:1769–85.

46. Oshi M, Takahashi H, Tokumaru Y, Yan L, Rashid OM, Nagahashi M, Matsuyama R, Endo I, Takabe K. The E2F Pathway Score as a Predictive Biomarker of Response to Neoadjuvant Therapy in ER+/HER2- Breast Cancer. Cells. 2020 Jul 8;9(7):1643.

47. Bacci M, Lorito N, Smiriglia A, Morandi A. Fat and Furious: Lipid Metabolism in Antitumoral Therapy Response and Resistance. Trends Cancer. 2021 Mar;7(3):198-213.

48. Leone RD, Powell JD. Metabolism of immune cells in cancer. Nat Rev Cancer. 2020 Sep;20(9):516-531.

49. Arner EN, Rathmell JC. Metabolic programming and immune suppression in the tumor microenvironment. Cancer Cell. 2023 Mar 13;41(3):421-433.

50. Pedrosa L, Foguet C, Oliveres H, Archilla I, de Herreros MG, Rodríguez A, Postigo A, Benítez-Ribas D, Camps J, Cuatrecasas M, Castells A, Prat A, Thomson TM, Maurel J, Cascante M. A novel gene signature unveils three distinct immune-metabolic rewiring patterns conserved across diverse tumor types and associated with outcomes. Front Immunol. 2022 Sep 2;13:926304.

51. Ma X, Bi E, Lu Y, Su P, Huang C, Liu L, Wang Q, Yang M, Kalady MF, Qian J, Zhang A, Gupte AA, Hamilton DJ, Zheng C, Yi Q. Cholesterol Induces CD8+ T Cell Exhaustion in the Tumor Microenvironment. Cell Metab. 2019 Jul 2;30(1):143-156.e5.

52. Harding JJ, Moreno V, Bang YJ, Hong MH, Patnaik A, Trigo J, Szpurka AM, Yamamoto N, Doi T, Fu S, Calderon B, Velez de Mendizabal N, Calvo E, Yu D, Gandhi L, Liu ZT, Galvao VR, Leow CC, de Miguel MJ. Blocking TIM-3 in Treatment-refractory Advanced Solid Tumors: A Phase Ia/b Study of LY3321367 with or without an Anti-PD-L1 Antibody. Clin Cancer Res. 2021 Apr 15;27(8):2168-2178.

53. Kelly RJ, Ajani JA, Kuzdzal J, Zander T, Van Cutsem E, Piessen G, Mendez G, Feliciano J, Motoyama S, Lièvre A, Uronis H, Elimova E, Grootscholten C, Geboes K, Zafar S, Snow S, Ko AH, Feeney K, Schenker M, Kocon P, Zhang J, Zhu L, Lei M, Singh P, Kondo K, Cleary JM, Moehler M; CheckMate 577 Investigators. Adjuvant Nivolumab in Resected Esophageal or Gastroesophageal Junction Cancer. N Engl J Med. 2021 Apr 1;384(13):1191-1203.

54. van den Ende T, de Clercq NC, van Berge Henegouwen MI, Gisbertz SS, Geijsen ED, Verhoeven RHA, Meijer SL, Schokker S, Dings MPG, Bergman JJGHM, Haj Mohammad N, Ruurda JP, van Hillegersberg R, Mook S, Nieuwdorp M, de Gruijl TD, Soeratram TTD, Ylstra B, van Grieken NCT, Bijlsma MF, Hulshof MCCM, van Laarhoven HWM. Neoadjuvant Chemoradiotherapy Combined with Atezolizumab for Resectable Esophageal Adenocarcinoma: A Single-arm Phase II Feasibility Trial (PERFECT). Clin Cancer Res. 2021 Jun 15;27(12):3351-3359.

FIGURE LEGENDS

Figure 1. Baseline higher immune gene signatures and reduced resistance to stress are associated with response to neoadjuvant chemotherapy.

A, Schematic overview of the study design showing our multidimensional analysis of pre-nCT tumor biopsies (by whole exome sequencing [WES], RNA sequencing [RNA-seq], immunohistochemistry [IHC], proteome digital spatial profiling [DSP], and

flow cytometry) and blood (flow cytometry, plasma cytokines) collected prospectively from patients diagnosed with locally advanced EAC (n=34); an additional cohort of archived pre-treatment EAC tumors (n=34) was analyzed by IHC and DSP. **B**, Hallmark gene set enrichment analysis comparison of complete responders (CRs, n = 9) vs. non-responders (NRs, n=9) showing normalized enrichment scores for gene sets with false discovery rates < 0.01. **C**, Volcano plot of genes enriched in CRs vs. NRs from bulk RNA-seq. The volcano plot reports the name of genes selected on the basis of their participation in pathways differentially enriched in GSEA analysis, as discussed in the Results. **D**, Oncoplot of somatic mutations in Reactome pathway MHC class I antigen processing and presentation genes, with respective percentages of mutated genes for each EAC sample. **E**, HLA loss-of-heterozygosity events represented as imbalanced HLA copy numbers observed in 2 patients, N 20 (PR) and N 8 (NR).

Figure 2. Increased baseline infiltration of $Foxp3^+$ and $CD163^+$ cells in EACs of non-responders is associated with reduced overall survival.

A, Cibersort scores for EAC-infiltrating immune cell populations were calculated from RNA-seq data for complete responders (CRs), partial responders (PRs), and non-responders (NRs). Bar graphs represent mean ± SEM; *p <0.05, **p <0.01, One-way ANOVA. Abbreviations for cell types: NV B = naïve B, ME B = memory B, P = plasma cells, CD8 = $CD8^+$, NV CD4 = naïve $CD4^+$, ME CD4 R = memory $CD4^+$ resting, ME CD4 A = memory $CD4^+$ activated, TFH = follicular T helper, TREG = T regulatory, γδT = gamma delta T, NK R = natural killer resting, NK A = natural killer activated, MONO = monocytes, M0 = M0 macrophages, M1 = M1 macrophages, M2 = M2 macrophages, DC R = dendritic cells resting, DC = dendritic cells activated,

MC R = mast cells resting, MC A = mast cells activated, EO = eosinophils, NEU = neutrophils. **B**, Representative immunostaining of pre-treatment EACs for Foxp3, CD163, and CD45RO; scale bar 50 μm. **C**, Staining scores for intra-tumoral (intra-Tum) and peri-tumoral regions (peri-Tum) in CRs (n=15), PRs (n=16), and NRs (n=33). Semiquantitative h scores (0 = no staining to 3 = strongest staining) were assigned by an expert pathologist. Data are presented as mean ± SEM; *p <0.05, one-way ANOVA. **D**, Overall survival of patients with high vs. low Foxp3 immunohistochemistry (IHC) staining scores in intra-tumor EAC infiltrates before neoadjuvant chemotherapy (high score, h ≥1; low score, h <1); *p <0.05, log-rank test. **E** and **F**, Overall survival of patients with high vs. low CD163 IHC staining scores in peri-tumoral (**E**) and intra-tumoral (**F**) EAC infiltrates before neoadjuvant chemotherapy (high score, h ≥2; low score, h <2); *p <0.05, **p <0.01, log-rank test.

Figure 3. Digital spatial profiling confirms distinct baseline functional immune contexture in EACs of complete responders and non-responders.

A, Experimental design: spatial proteomic profiling of 53 tumor and immune markers was conducted on formalin-fixed and paraffin-embedded EAC biopsy sections; selection of multiple regions of interest (ROIs) per tissue sample was based on immunofluorescent staining for PanCK (tumor epithelial marker), CD68 (macrophages), and CD3 (T lymphocytes); nuclei were stained with DAPI. Protein counts were measured within $PanCK^+$-enriched tumor regions (masks) and $PanCK^-$ stromal regions (inverted masks). **B**, Volcano plot of proteins enriched in $PanCK^+$ (n=72) vs. $PanCK^-$ (n=72) areas showing statistical significance for proteins with p <0.05; p-values were calculated using the linear mixed model (LMM). **C**, Representative immunofluorescent staining for PanCK, CD68, and CD3 in tumor

tissue from complete responders (CRs) and non-responders (NRs); scale bar 100 µm. **D**, CD3 PanCK$^+$/PanCK$^-$ ratios for each ROI (normalized by area) for CRs and NRs (calculated from digital spatial profile reads); *p <0.05, unpaired t-test. **E** and **G**, Volcano plots of proteins enriched in PanCK$^-$ (**E**) and PanCK$^+$ (**G**) areas in tumors from CRs (n=33 ROIs) vs. NRs (n=39 ROIs), showing statistical significance for proteins with p <0.05; p-values were calculated using the LMM. **F** and **H**, Corresponding box plots representing read numbers (N) normalized to the area for proteins differentially enriched in PanCK$^-$ (**F**) and PanCK$^+$ areas (**H**), presented as mean ± SEM; *p <0.05, **p <0.01, unpaired t-test.

Figure 4. Responder EACs show reduced baseline infiltration of Foxp3$^+$ Tregs and an increased frequency of tissue-resident CD8$^+$CD39$^+$ T cells.

A, Representative flow cytometry plots of tumor single-cell suspensions (CD3$^+$ viable cells) stained for 9 surface markers, showing the gating strategy for CD25$^+$CD127^{low} T regulatory-like cells (Tregs) and CD8$^+$CD39$^+$CD103$^+$ T cells. **B** and **C**, Dot plots showing frequencies expressed as % of CD25$^+$CD127^{low} CD4$^+$ cells (**B**) and CD39$^+$CD103$^+$ CD8$^+$ cells (**C**) in pre-treatment EAC tumor cell suspensions from complete responders (CRs, n=9) and non-responders (NRs, n=6), determined by manual gating. Data are presented as mean ± SEM; *p <0.05, unpaired t-test. **D**, Exemplified tSNE visualization of 17 surface markers representing 6,000 merged CD3$^+$CD4$^+$ cells in tumor cell suspensions from CRs (n=3) and NRs (n=3); 13 clusters were predicted by unsupervised PhenoGraph analysis. **E**, Histograms showing the expression of 6 surface markers in clusters #4 and #5, concatenated CD3$^+$CD4$^+$ events (Conc), and negative control (Neg); relative fluorescence intensity (RFI) values are shown. **F**, Exemplified tSNE visualization of 17 surface markers

representing 6,000 merged $CD3^+CD8^+$ cells in tumor cell suspensions from CRs (n=3) and NRs (n=3); 11 clusters were predicted by unsupervised PhenoGraph analysis. **G**, Histograms showing the expression (RFI values) of 12 surface markers in clusters #1 and #2, concatenated $CD3^+CD8^+$ events (Conc), and negative control (Neg). **H**, Exemplified tSNE visualization of 8 markers, including 3 surface markers and 5 nuclear transcription factors, representing 6,000 merged $CD3^+CD4^+$ cells in tumor cell suspensions from CRs (n=3) and NRs (n=3); 9 clusters were predicted by unsupervised PhenoGraph analysis. **I**, Histograms showing the expression (RFI values) of 7 markers in cluster #6, ($CD25^+CD127^{low}Foxp3^+$ Treg-like cells), concatenated (Conc) $CD3^+CD4^+$ events, and negative control (Neg). **J**, Exemplified tSNE visualization of 8 markers (3 surface markers and 5 nuclear transcription factors), representing 6,000 merged $CD3^+CD4^-$ cells in tumor cell suspensions from CRs (n=3) and NRs (n=3); 9 clusters were predicted by unsupervised PhenoGraph analysis. **K**, Histograms showing the expression (RFI values) of 8 markers in cluster #3, concatenated $CD3^+CD4^-$ events (Conc), and negative control (Neg).

Figure 5. Non-responder EACs show increased baseline infiltration of pro-tumor M2-like macrophages.

A, Exemplified tSNE visualization of 20 surface markers representing 7,000 merged $CD45^+CD3^-$ tumor cells from complete responders (CRs, n=3) and non-responders (NRs, n=4); cells are colored according to the 10 clusters assigned by PhenoGraph and manual annotation; the corresponding heatmap shows median marker intensity normalized to a 0–1 range. **B**, Frequencies of the clusters in CR (n=3) and NR (n=4) $CD45^+CD3^-$ cells presented as mean ± SEM; *p <0.05, one-way ANOVA. **C**, Histograms showing the expression of 6 surface markers in cluster #3 (assigned as

M2-like macrophages), concatenated $CD45^+CD3^-$ events (Conc), and negative control (Neg); relative fluorescence intensity (RFI) values are shown.

Figure 6. Increased frequency of circulating exhausted T cells and myeloid-derived suppressor cells in non-responders to neoadjuvant chemotherapy prior to treatment. **A**, Exemplified tSNE visualization of 17 surface markers representing 32,000 merged $CD3^+CD4^+$ cells peripheral blood mononuclear cells (PBMCs) from complete responders (CRs, n=8) and non-responders (NRs n=8) before neoadjuvant chemotherapy; 18 clusters were predicted by unsupervised PhenoGraph analysis. **B**, Histograms showing the expression of 6 markers in cluster #6 (T effector memory $KLRG1^{high}PD1^{high}$), concatenated $CD3^+CD4^+$ events (Conc), and negative control (Neg); relative fluorescence intensity (RFI) values are shown. **C**, Exemplified tSNE visualization of 17 surface markers representing 16,000 merged $CD3^+CD8^+$ pre-nCT PBMCs from CRs (n=8) and NRs (n=8); 14 clusters were predicted by unsupervised PhenoGraph analysis. **D**, Histograms showing the expression (RFI values) of 6 markers in cluster #8 (T transitional memory $TIGIT^{high}$ $PD1^{high}$), concatenated $CD3^+CD8^+$ events (Conc), and negative control (Neg). **E**, Exemplified tSNE visualization of 20 surface markers representing 15,000 merged $CD45^+CD3^-$ pre-nCT PBMCs from CRs (n=7) and NRs (n=8). Cells are colored according to the 11 clusters assigned by PhenoGraph and manual annotation; the corresponding heatmap shows median marker intensity normalized to a 0–1 range. **F**, Histograms showing the expression (RFI values) of 5 surface markers in PhenoGraph clusters #1 and #4, concatenated $CD45^+CD3^-$ events, and negative control (Neg); clusters #1 and #4 were assigned as monocytes HLA-DR^{high} (enriched in CRs) and MO-MDSC $CCR7^+$ (enriched in NRs), respectively. **G**, Frequencies of $CD45^+CD3^-$ cells in 11

PhenoGraph clusters (determined by 20 surface markers) in CRs (n=7) and NRs (n=8), presented as mean ± SEM; **p < 0.01, one-way ANOVA. H. Correlation between the flow cytometry frequency (%) of $CD14^{+}HLA\text{-}DR^{high}$ PBMCs and $CD39^{+}CD103^{+}CD8^{+}$ TILs for n=12 patients; 95% confidence interval is shaded in gray. R; Spearman's correlation; p=p value.

Figure 7. Differential circulating pro-inflammatory cytokines and complement anaphylatoxins in responders and non-responders to neoadjuvant chemotherapy.

A, Baseline plasma concentrations of GM-CSF, IL-4, CXCL10, C3a, and C5a in complete responders (CRs, n = 12) and non-responders (NRs, n = 14); bars represent mean ± SEM, *p < 0.05, **p <0.01, unpaired t-test. **B**, Spearman's correlation coefficients for the 30 circulating cytokines analyzed and frequency of tumor-infiltrating $CD8^{+}CD39^{+}CD103^{+}$ cells (calculated by flow cytometry manual gating on 15 baseline EACs); *p < 0.05, **p < 0.01. **C**, Correlation between the baseline plasma concentration of RANTES, IL1RA, GM-CSF, and IL-4 and flow cytometry frequency (%) of $CD39^{+}CD103^{+}CD8^{+}$ TILs for n=15 patients; 95% confidence interval is shaded in gray. R; Spearman's correlation; p=p value. **D**, Correlation between the baseline plasma concentration of GM-CSF and flow cytometry frequency (%) of circulating $CD14^{+}HLA\text{-}DR^{high}$ cells for n=15 patients; 95% confidence interval is shaded in gray. R; Spearman's correlation; p=p value.

Figure 1

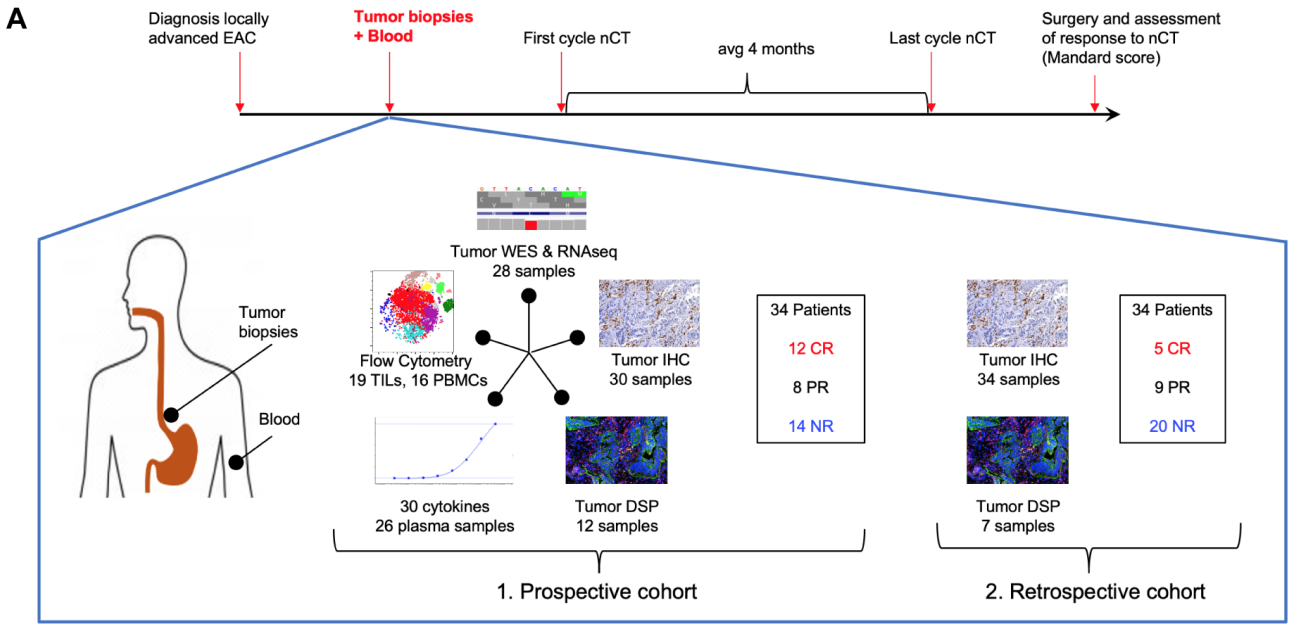

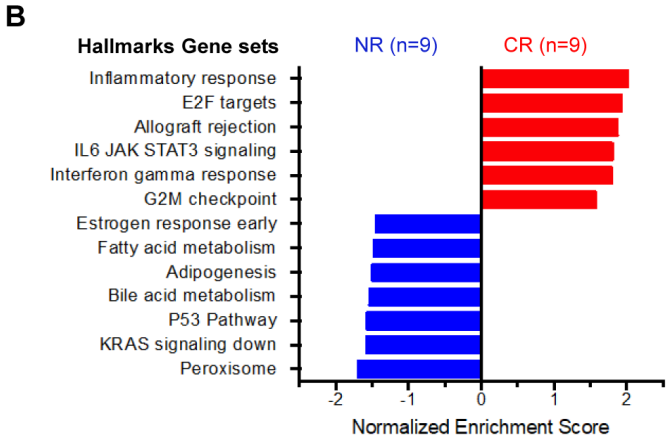

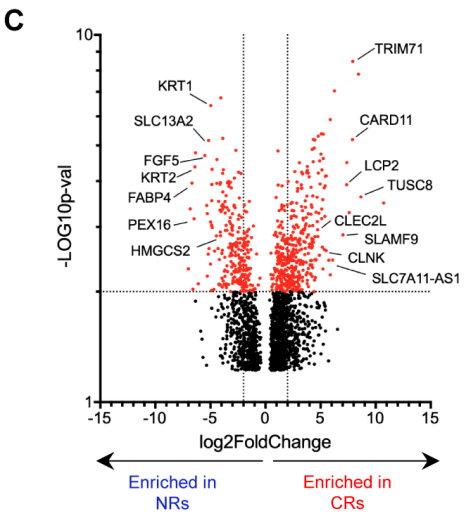

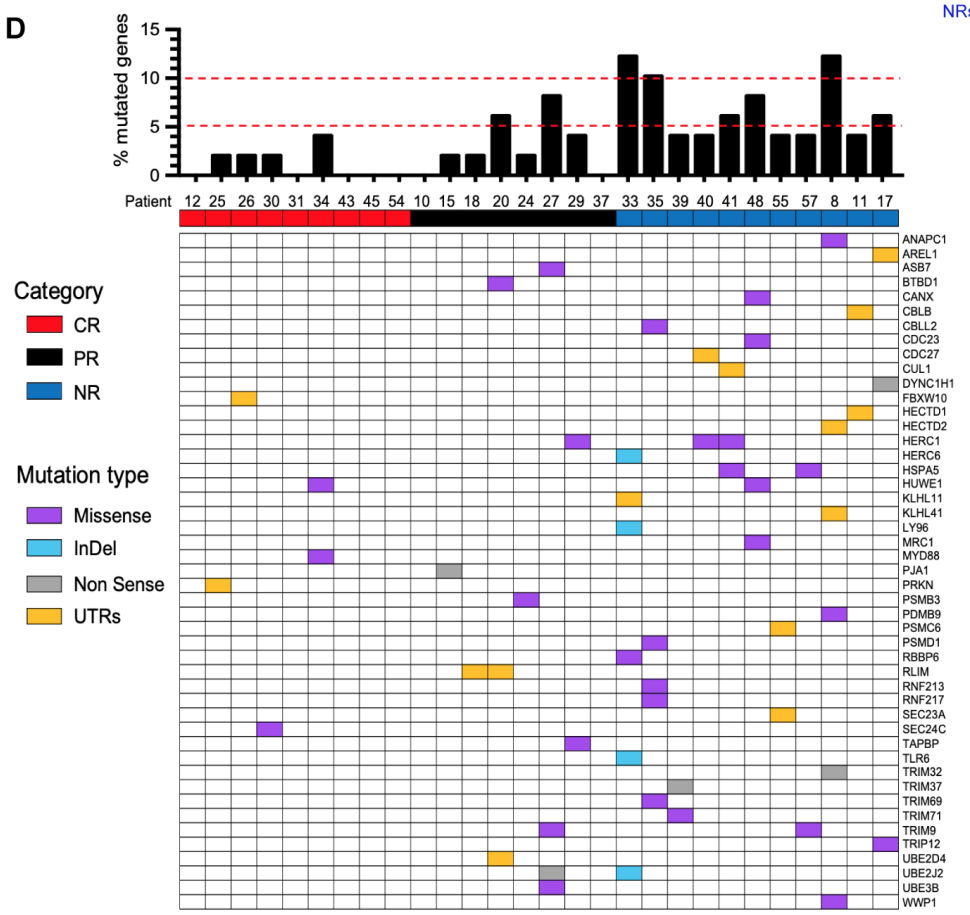

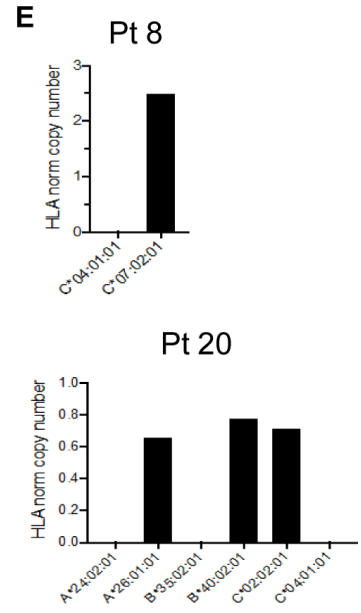

Figure 2

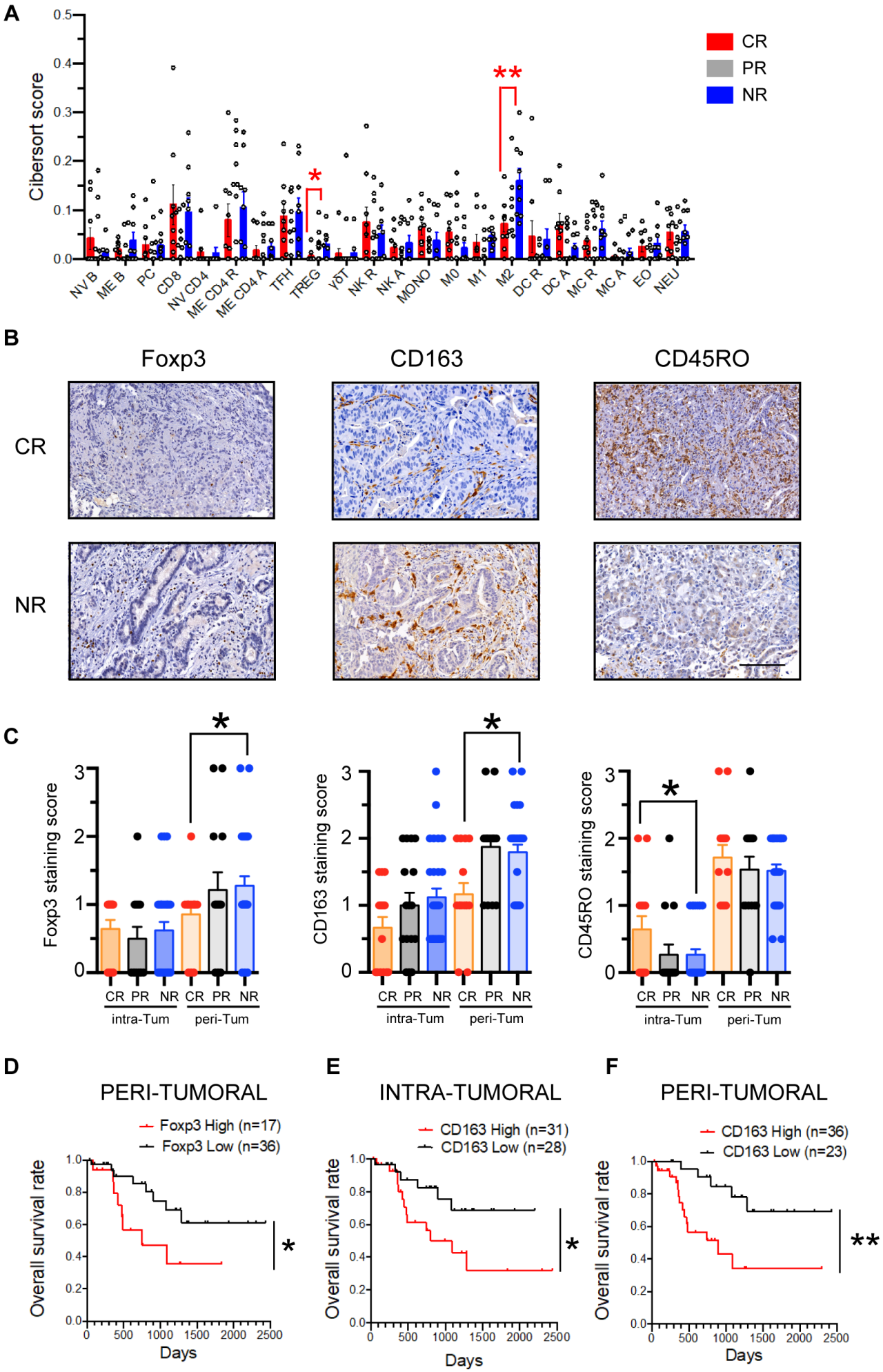

Figure 3

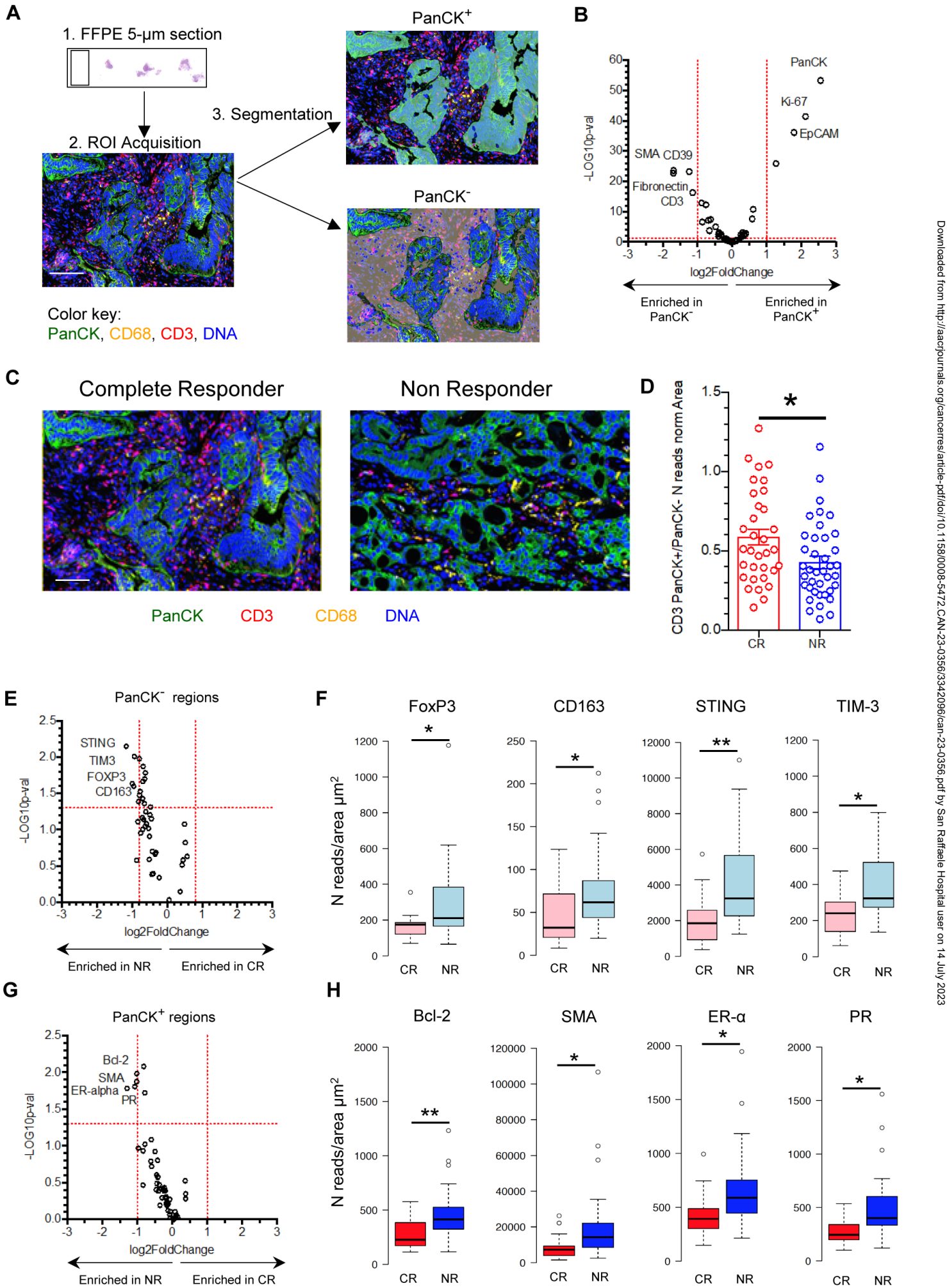

Figure 4

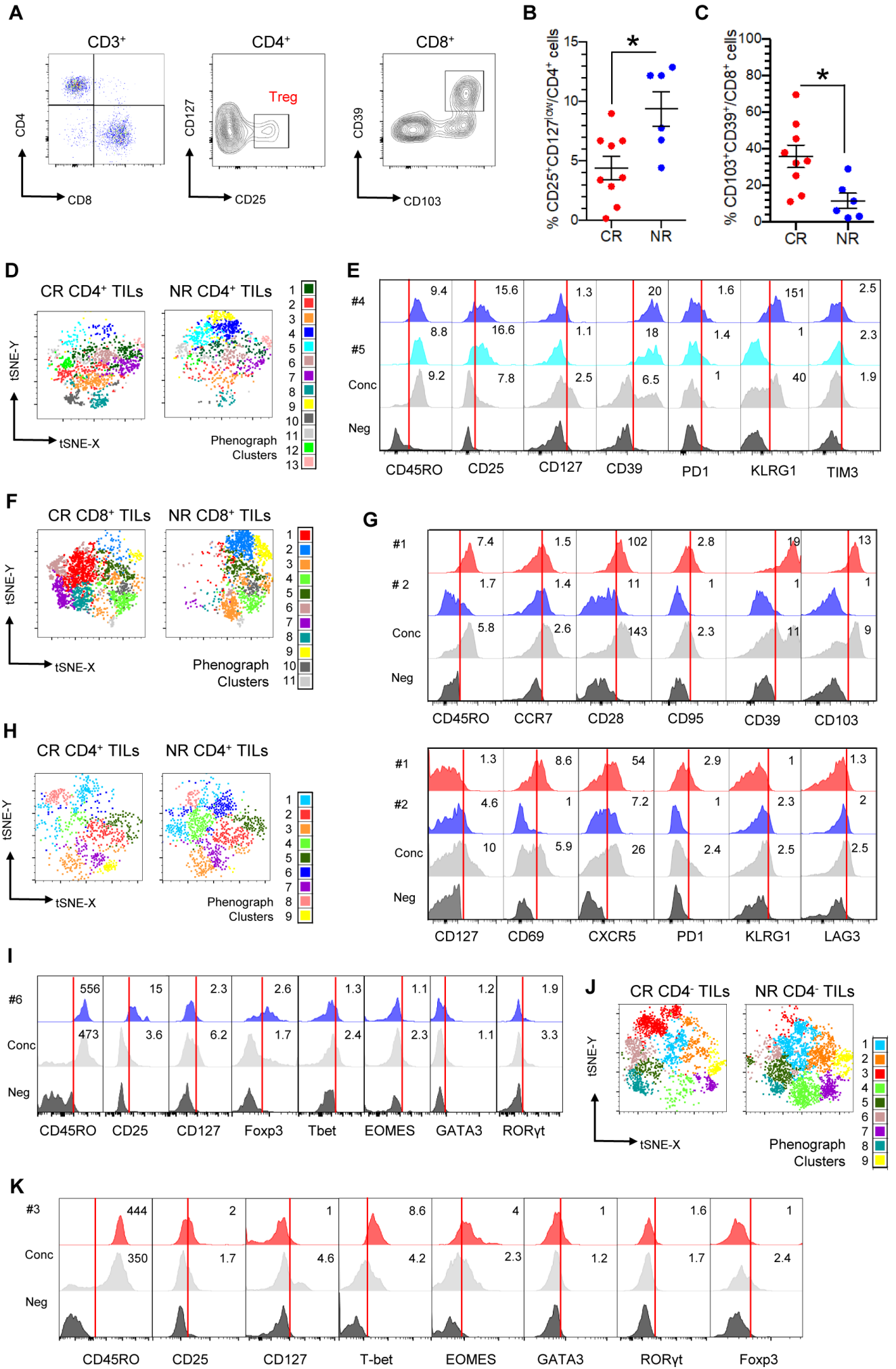

Figure 5

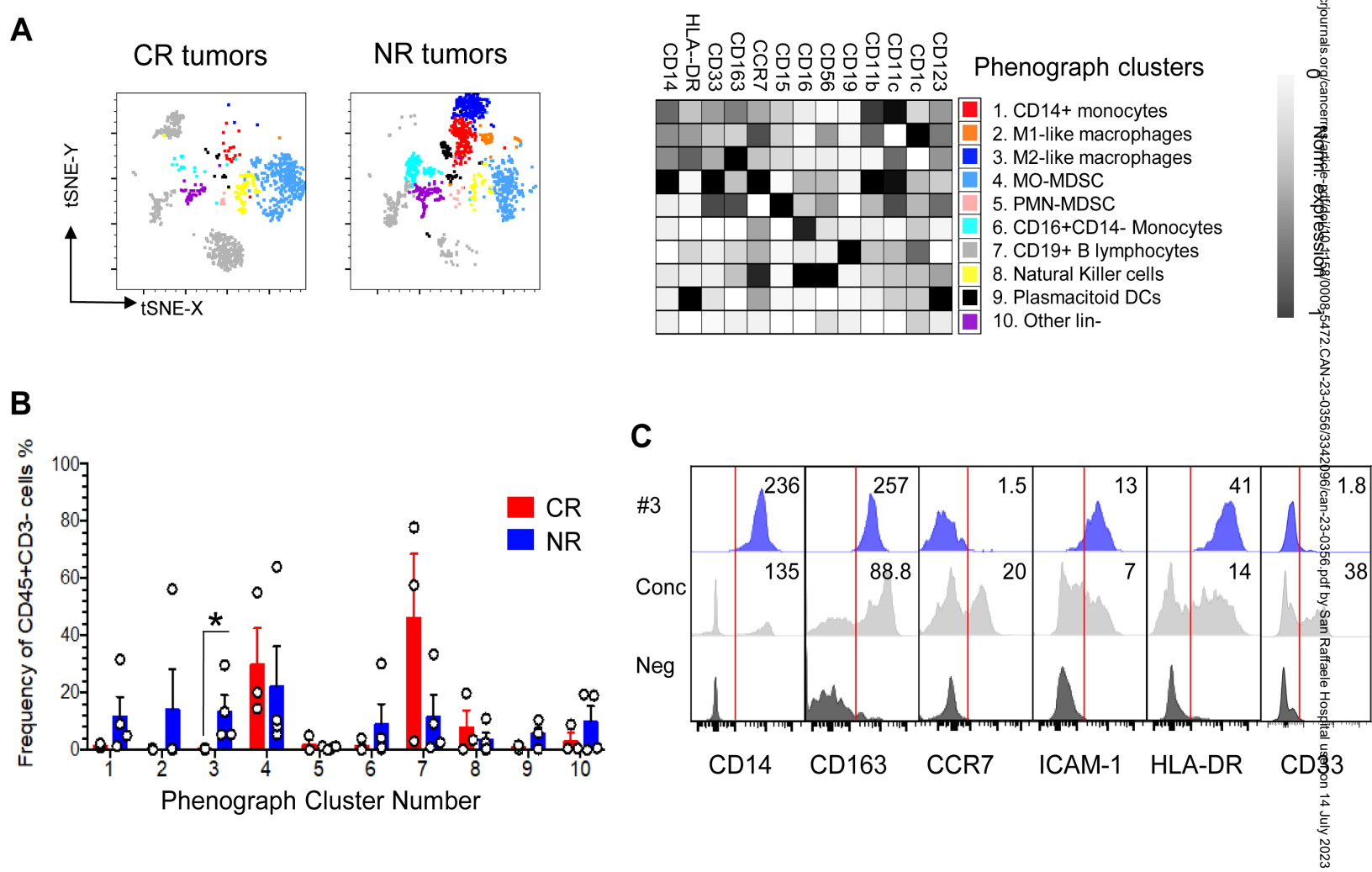

Figure 6

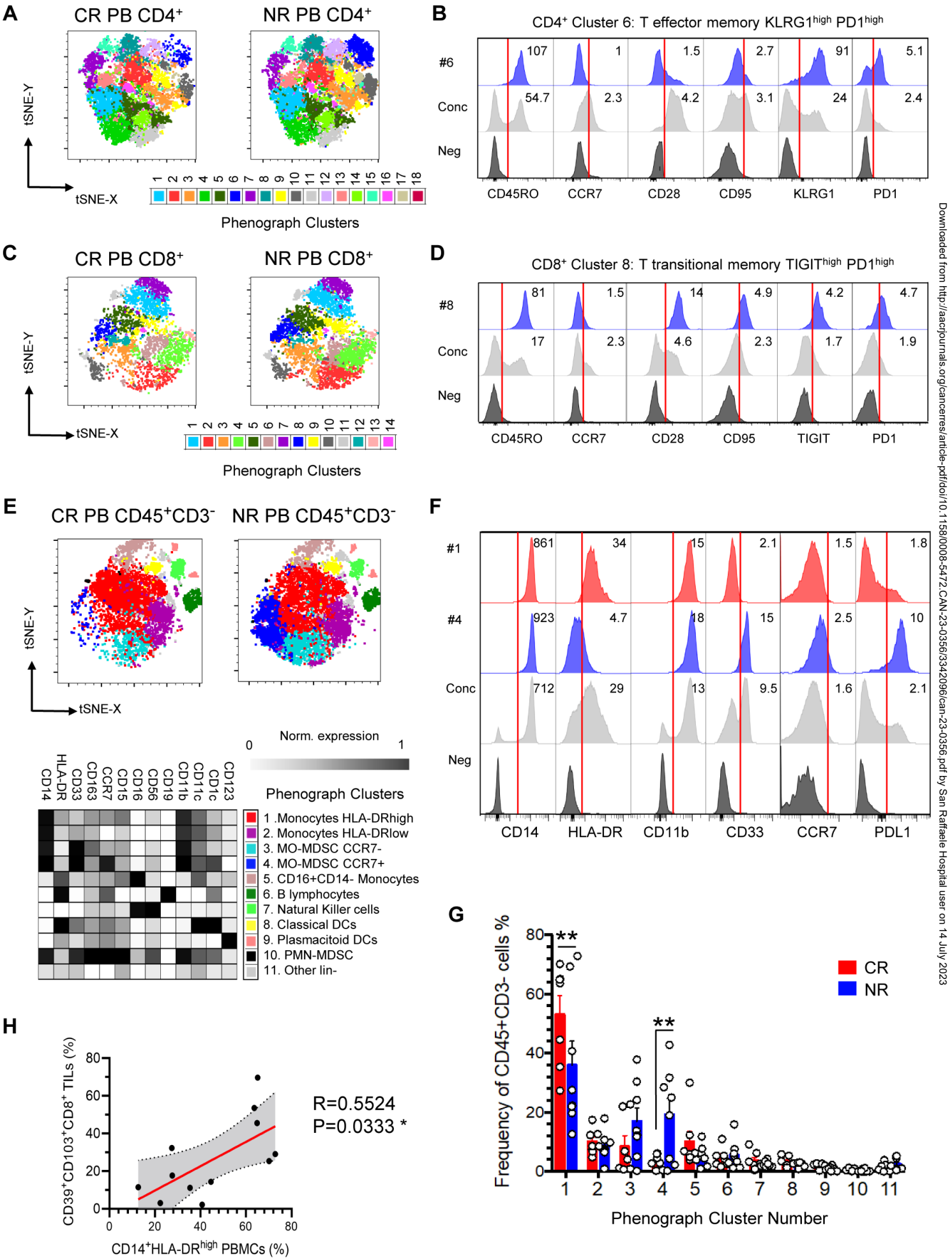

Figure 7